Particuology 10 (2012) 542–552

Contents lists available at SciVerse ScienceDirect

Particuology

journal homepage: www.elsevier.com/locate/partic

Discrete element modeling of inherently anisotropic granular assemblies with polygonal particles

Ehsan Seyedi Hosseininia*

Civil Engineering Department, Faculty of Engineering, Ferdowsi University of Mashhad, Mashhad, Iran

ARTICLE INFO

Article history:
Received 22 August 2011
Received in revised form 12 October 2011
Accepted 24 November 2011

Keywords:
Inherent anisotropy
Granular material
Discrete element method
Polygonal particles

ABSTRACT

In the present article, we study the effect of inherent anisotropy, i.e., initial bedding angle of particles and associated voids on macroscopic mechanical behavior of granular materials, by numerical simulation of several biaxial compression tests using the discrete element method (DEM). Particle shape is considered to be irregular convex-polygonal. The effect of inherent anisotropy is investigated by following the evolution of mobilized shear strength and volume change during loading. As experimental tests have already shown, numerical simulations also indicate that initial anisotropic condition has a great influence on the strength and deformational behavior of granular assemblies. Comparison of simulations with tests using oval particles, shows that angularity influences both the mobilized shear strength and the volume change regime, which originates from the interlocking resistance between particles.

1. Introduction

Granular materials consist of discrete particles and associated voids and therefore, the response of such a particulate medium highly depends on the individual characteristics of particles such as shape and angularity as well as the overall properties of the assembly such as alignment and spatial arrangement of grains. The latter particularly pertains to soil anisotropy. Practically, all soil structures, natural or man-made, are influenced by gravitational field which induces an anisotropic soil fabric. During deposition of soil particles, similar to what happens in river, beach or coastal sand dunes or in artificially deposited sand layers, particles tend to be aligned in some preferred direction, thus generating an initial inherent anisotropy in the soil structure, which eventually affects engineering properties of the granular soils, such as bearing capacity and deformational characteristic.

This matter has been the subject of several experimental studies in laboratory. Arthur and Menzies (1972) and Oda (1972) by performing triaxial compression tests, and Oda, Koishikawa, and Higuchi (1978) by carrying out plane strain tests on sand, showed that particle alignment has a significant effect on shear strength. They found that shear strength is the highest for samples, in which the major principal stress axis is perpendicular to the bedding plane (the direction of the long side of particles with respect to the horizontal) of the sand particles. Later, Miura, Miura, and Toki (1986) conducted a series of drained tests on inherently anisotropic sand samples using a hollow cylinder torsional shear apparatus, to investigate the shear strength and deformational characteristics under loading conditions including fixed and continuous rotational principal stress axes. They concluded that the effects of initially anisotropic fabric on both shear strength and volume change behavior are especially significant. They also explained that the anisotropic deformational characteristic is uniquely caused by the predominant sliding occurring on the bedding plane, irrespective of any rotation of the principal stress axes. In addition to tests on real sands, Oda, Nemat-Naser, and Konishi (1985) performed several biaxial compression tests on two-dimensional assemblies of oval cross-sectional rods, focusing on the evolution of contact formation between particles as well as particle rotation which was found to be inclined toward the major principal direction. This is referred to as induced anisotropy. Moreover, these authors showed that elongated voids were generated along the major principal direction which seems to be a contributing factor to post-peak failure as well as dilative behavior of the granular material.

In addition to such experimental works, other attempts have also been made to incorporate inherent anisotropy within the framework of the plasticity theory of granular soils (Dafalias, Papadimitriou, & Li, 2004; Oda, 1993) as well as numerical simulations using the discrete element method (DEM), which led to attempts to study inherent anisotropy. For example, Ting and Meachum (1995) numerically investigated the inherent anisotropy in an assembly with ellipse-shaped particles under

* Tel.: +98 511 8805111; fax: +98 511 8763303; mobile: +98 912 2263498.
E-mail address: eseyedi@um.ac.ir

1674-2001/$ – see front matter
http://dx.doi.org/10.1016/j.partic.2011.11.015

monotonic loading. Ng (2004) studied the effect of stress path and the intermediate principal stress on samples with different degrees of anisotropy using ellipsoid particles. Recently Sazzad and Suzuki (2010) addressed the effect of inherent anisotropic fabric on the evolution of micro-behavior of assemblies with oval-shaped particles under cyclic loading. And Mahmood and Iwashita (2010) investigated, too, the influence of inherent anisotropy on stress–strain behavior of shear band formation by performing biaxial plain strain tests using oval/elliptical-shaped particles. All these studies signify in general that inherent anisotropy plays an important role in the mechanical behavior of granular media including shear strength and volume change response.

Referring to numerical studies of granular aggregates oriented to inherent anisotropy, it was found that all DEM simulations were performed by using oval/ellipsoidal particles, although particles in granular soils, such as sand, are by no means ellipsoidal in shape, but consist of irregular polygons. However, the form of grains, such as angularity or roundness, significantly influences the soil mechanical behavior. Experimental research (Bowman, Soga, & Drummond, 2011; Houlubec & D'Appolonia, 1973) as well as numerical studies using DEM (Mirghasemi, Rothenburg, & Matyas, 1997; Peña, García-Rojo, & Herrmann, 2007; Pudasaini & Hutter, 2007; Shodjaa & Nezami, 2003) indicated that assemblies with elongated and sharp edged particles show greater shear strength and dilatancy, due to interlocking among particles, which affects the process of shear strength mobilization.

The objective of the present paper is to investigate the effect of inherent anisotropy on the mechanical response of granular assemblies, consisting of two-dimensional (2D) polygon-shaped particles by using DEM. This work purports to verify DEM simulations in which, inherent anisotropy is investigated by employing oval/ellipsoidal particles. This is achieved by a comparative study between experimental tests and numerical simulations. Four biaxial compression tests on granular assemblies are simulated and the results are discussed in terms of shear strength and volume change.

2. Numerical modeling

The numerical modeling in this paper involves simulations using 2D models. This simplification could be considered as an imperfection of this study since in reality, granular particles are always 3D. However most key phenomena and behavior based on microstructural mechanisms in reality could be successfully captured by 2D models (Oda, Kazama, & Konishi, 1998; Oda, Konishi, & Nemat-Nasser, 1982; Oda et al., 1985), while 3D models is by far more expensive and more elaborate analyses are needed. In fact, the primary goal of 2D simulations is to orient the study of granular materials toward the correct direction. The 2D findings could later be evaluated by future experimental tests on real materials as well as by performing 3D simulations.

In the domain of numerical simulations using DEM, several ideas can be found in order to model irregularly shaped particles. For instance, some efforts were made on creating non-circular/spherical particles by considering clusters of bonded circles/spheres (Jensen, Bosscher, Plesha, & Edil, 1999) or overlapping rigid clusters (Sallam, 2004). Although clustering techniques can provide angular particles for more rigorous simulations, they would require a large amount of memory thus increasing calculation time. The approach used in the present study, considers each particle as an individual convex polygon (Mirghasemi et al., 1997; Peña et al., 2007). By this approach, it is possible to predefine the geometry of particles as an arbitrary convex polygon. As a consequence, simulation is simple and efficient as compared to the clustering techniques.

The principle and the procedure of numerical simulation of a granular medium in the present paper are first briefly explained. Simulation is performed by using the program POLY (Mirghasemi et al., 1997) based on the numerical discrete element method (DEM). This program is a version of the code DISC (Bathurst, 1985) modified to simulate assemblies of two-dimensional arbitrary shaped convex polygons. It is noted that this code has already been evaluated for simulating granular media (Mirghasemi, Rothenburg, & Matyas, 2002) and later modified to simulate the breakage and fragmentation of polygon-shaped particles (Seyedi Hosseininia & Mirghasemi, 2006, 2007).

2.1. Principles of DEM simulation

DEM is based on dynamics formulations. However, DEM simulation used for studying mechanical properties of soils deals with pseudo-static problems rather than impact and dynamic problems such as avalanche and rapid granular flow (Peña, McNamara, Lind, & Herrmann, 2009; Pudasaini, 2011; Pudasaini et al., 2007; Teufelsbauer, Wang, Pudasaini, Borja, & Wu, 2011). Hence, load and displacement rates are small enough that moderate variation does not significantly influence simulation results.

In DEM, each particle is considered as a rigid body which can move and rotate due to applied external forces and moments from adjacent particles. In a Cartesian coordinate system (1–2), for each individual particle, both rotational and translational accelerations of motion are calculated in every time step during the simulation process by using Newton's second law of motion:

$$\begin{aligned} (I\ddot{\theta})_N &= \left(\sum M\right)_N, \\ (m\ddot{X}_i)_N &= \left(\sum F_i\right)_N, \end{aligned} \tag{1}$$

where m and I are the mass and moment of inertia of the particle N, respectively; F_i and M are the ith force component and the moment applied at the center of gravity of the particle N, respectively. No gravitational force (weight) is considered in the simulation. Since force components ($i = 1, 2$) are applied on the periphery of the particle, a moment is considered for the particle due to transfer of the force components to the center of gravity; $\ddot{X}_i$ and $\ddot{\theta}$ stand for translational and rotational accelerations of the particle N, respectively. These equations are integrated once to calculate the respective velocity and then again to find the displacement and rotational components.

For each particle, extra force and moment components are defined in order to consider viscous translational and rotational damping. The damping force, F_i^{D}, and the damping moment, M^{D}, are related to the translational ($\dot{X}_i$) and rotational ($\dot{\theta}$) velocity components by constants C_{m} and C_{I} as follows:

$$\begin{aligned} F_i^{\mathrm{D}} &= -C_{\mathrm{m}}\dot{X}_i, \\ M^{\mathrm{D}} &= -C_{\mathrm{I}}\dot{\theta}, \end{aligned} \tag{2}$$

where $C_{\mathrm{m}} = \alpha_{\mathrm{m}} m$ and $C_{\mathrm{I}} = \alpha_{\mathrm{I}} I$, in which α_{m} and α_{I} are damping coefficients.

2.2. Contact law

The contact model used in the simulation is similar to what was introduced by Mirghasemi et al. (1997) and Peña et al. (2007). Fig. 1 presents the configuration of the contact between two particles. The points P_1 and P_2 represent the intersection points of polygons. The length of line $\overline{P_1P_2}(L)$ is used to define the deformation length $\delta = A/L$, where A is the overlap area between particles. For each contact, a contact force comprises normal and tangential components.

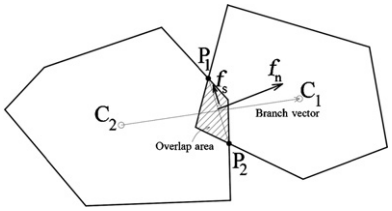

Fig. 1. Schematic representation of the contact between two polygon particles as characterized by the overlap area between two contacting particles.

The direction of the normal contact force (f_n) is perpendicular to the line $\overline{P_1P_2}$ and the value is calculated as follows:

$$f_n = k_n\delta, \tag{3}$$

where k_n is normal stiffness coefficient. Similarly, the tangential contact force (f_s) exerted along the line $\overline{P_1P_2}$, is defined as:

$$f_s = k_s\Delta, \tag{4}$$

where k_s is shear stiffness coefficient and Δ is the relative tangential displacement of two particles along the line $\overline{P_1P_2}$. Although the normal contact force is repulsive and elastic, the contact force along the line $\overline{P_1P_2}$ (the tangential contact force) is considered frictional in such a way that sliding occurs when $|f_s| > \mu_s f_n$. Otherwise, the relationship between shear force and tangential displacement is recoverable. μ_s equals $\tan\phi_\mu$. ϕ_μ is the inter-particle friction angle, which relates to the characteristics of particles material (Lambe & Whitman, 1969).

2.3. Stress and strain tensors

In a Cartesian coordinate system (1–2), the average stress tensor (σ_{ij}) acting on a granular assembly can be computed (Christoffersen, Mehrabadi, & Nemat-Nasser, 1981; Rothenburg & Selvadurai, 1981) as:

$$\sigma_{ij} = \frac{1}{V}\sum_{\alpha=1}^{N_c} f_i^\alpha l_j^\alpha, \quad i,j = 1,2 \tag{5}$$

where V denotes the volume of the assembly; f_i^α is the ith component of the contact force acting at the αth contact point between two particles; l_j^α is the jth component of the branch vector connecting the centroids of two particles forming the αth contact force f^α; N_c is the total number of contact points in the volume V.

If external forces $T_i^1, T_i^2, \ldots, T_i^m$ are exerted on the boundary points $x_i^1, x_i^2, \ldots, x_i^m$, the average stress tensor of an assembly with statically balanced condition can also be assessed by (Bathurst, 1985):

$$\sigma_{ij} = \frac{1}{V}\sum_{\beta=1}^{m} T_i^\beta x_j^\beta, \quad i,j = 1,2 \tag{6}$$

The average strain tensor (ε_{ij}) of an assembly with the volume V can be obtained by measuring displacements of boundary particles as follows (Cundall & Strack, 1979):

$$\varepsilon_{ij} = \frac{1}{V}\sum_{\beta=1}^{N_b}\left[\frac{1}{2}\{\Delta x_j^\beta + \Delta x_j^{\beta+1}\}e_i^\beta S^\beta\right], \quad i,j = 1,2 \tag{7}$$

The boundary is defined by connecting the centers of all boundary particles to one another. According to Fig. 2, Δx_j^β and $\Delta x_j^{\beta+1}$ represent the jth components of the displacements of two adjacent particles, connected to each other through line S^β; e_i^β is the ith component of the unit vector whose direction is perpendicular to S^β; N_b is the number of total boundary contact points.

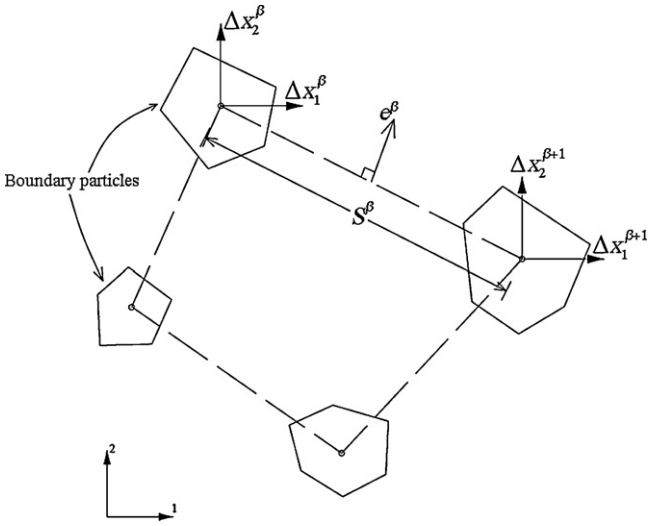

Fig. 2. Definition of average strain tensor by considering displacements of boundary particles. The boundary of the assembly is recognized by S^β segments connecting the centers of boundary particles.

3. Numerical simulations

3.1. Generation of particles

The geometry of the polygons considered as the particle shape can be arbitrarily chosen in the current numerical procedure and there is no limitation in the shape except for being convex. The polygon is defined by arbitrary number of edges and sizes. In the present study, three forms of particles with three different sizes are considered for numerical specimens. The size of particles is taken similar to that mentioned by Mahmood and Iwashita (2010), where the particles were oval/ellipsoidal in shape. Moreover, the geometry of each particle is considered in such a way that the polygon can fit inside an ellipse, as depicted in Fig. 3. Considering such similarity in the size and geometry provides a better condition to compare the results. The aspect ratio (the ratio of the major axis to the minor axis of the ellipse) of all particles is 1.5. The particle sizes represented by the major axis length range from 4.5 to 7.5 mm, as depicted in Table 1.

3.2. Preparation of numerical specimens

In order to study the effect of inherent anisotropy on the behavior of granular assemblies, four dense samples with different initial bedding angles (particle inclination from the horizontal direction) $\alpha = 0^\circ, 30^\circ, 60^\circ$, and 90° are considered. The initially generated space for 2-D specimens is a circle with diameter of 160 mm. Hence, the ratio of the sample diameter to the largest particle size is 21.3. By comparing this ratio with the value of 10, which is mentioned in BS1377-7 standard for shear box apparatus, it is obvious that the

Table 1
Dimensions of different types of particles.

Description	Dimension B(mm) × L(mm)	Particle type[a]
Small size	3.0 × 4.5	I, II, III
Medium size	4.0 × 6.0	I, II, III
Large size	5.0 × 7.5	I, II, III

[a] For geometry of particle types, refer to Fig. 3.

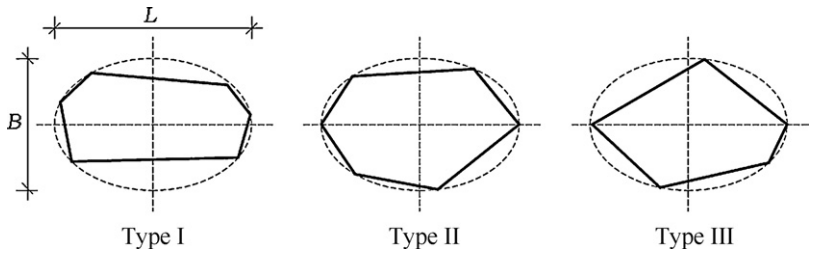

Fig. 3. Three types of particle geometry used in the present numerical simulations. Three different sizes are considered for each particle type according to Table 1.

sample diameter is large enough in order to avoid the effect of particle size on test results. Within each sample, about 2000 particles can be stacked. The number of each particle type is defined by introducing one frequency distribution (in terms of percentage) for all four samples. The frequency distribution is characterized by the uniformity coefficient (D_{60}/D_{10}) of 1.35 and the curvature coefficient ($D_{30}^2/D_{10}D_{60}$) of 1.2. D_x indicates the diameter of soil particles for which x% of the particles are finer.

In DEM-based simulations, the common method to prepare inherent anisotropic granular specimens with a specific bedding angle is to use the gravity deposition method (e.g., Ng, 2004; Nouguier-Lehon, Cambou, & Vincens, 2003), which is similar to the preparation of pluviation sand samples in experimental studies (e.g., Al-Hattamleh, Muhunthan, & Shalabi, 2009; Arthur & Menzies, 1972; Arthur & Phillips, 1975). In the present study, another numerical procedure is taken into consideration to prepare the assemblies with desired bedding angle. As explained before, the number of required particles for each type is firstly determined based on the introduced particle type distribution and then, each particle is placed inside the prescribed space randomly under the condition that the particle does not overlap previously laid particles and that the major axis of the particle is in the defined direction, i.e., bedding angles of $\alpha = 0^\circ$, 30°, 60°, and 90° from the horizontal.

Fig. 4(a) shows the initially generated sample with bedding angle of 30°. The assembly is characterized by interior particles confined by a series of boundary particles which are highlighted in the figure. As mentioned before, the center of each boundary particle represents the vertex of a convex polygon comprising straight-line segments joining boundary particle centers. At each calculation step, force or velocity (displacement rate) is applied to the center of each boundary particles. As the system deforms, the boundary particles are updated. If the center of an interior particle intercepts any straight-line of boundary segments, that particle becomes a boundary particle. A more detailed scheme for identifying boundary particles in the assembly is described elsewhere (Sitharam, 1991).

This initially generated assembly is sparse. Thus, as the second stage of sample preparation, the sample is isotropically consolidated in order to reduce large spatial voids. This compaction is achieved by pushing the boundary particles toward the center of the assembly. At this stage, the particles are allowed to move freely in the assembly so that a dense sample can be obtained. However, a high value is intentionally chosen for the rotational damping coefficient in order to effectively retain the initial orientation of particles (see, e.g., Sazzad & Suzuki, 2010). The consolidation continues until a very small stress is generated in the assembly, which means the end of initial consolidation. In addition, the inter-particle friction angle (ϕ_μ) is intentionally set to zero to facilitate compaction. However, as shown by Pudasaini and Kröner (2008), the inter-particle friction parameter (ϕ_μ) can play a very important role in properly modeling the granular flow dynamics, deposition and compaction in deposition. The last stage of sample preparation before it is loaded in biaxial compression test, consists of further isotropic consolidation though in a different manner, that is, the sample is compacted in a number of cycles under constant isotropic pressure until a steady-state volume contraction is reached, so that no further reduction in void occurs. The confining pressure for all samples is considered to be 300 kPa. Fig. 4(b) shows the final isotropically compacted specimen with $\alpha = 30^\circ$, ready for shear loading. Fig. 5 shows the evolution of void ratio (e) of all specimens during the compaction process. Since particle distribution and confining pressure of all particles are the same, the final void ratios obtained are close to each other at the end of isotropic consolidation ($0.25 < e < 0.26$). Such low values of void ratios only pertain to 2D models, and the measured void ratios for real sand samples are higher. Hereafter, each sample is ready for biaxial shear test. It

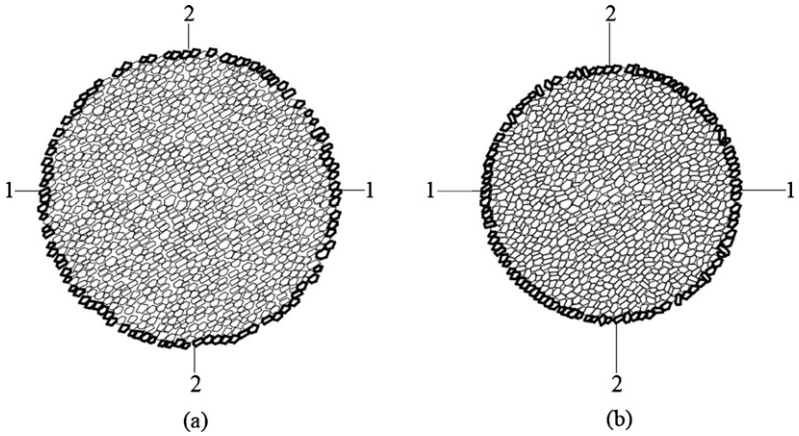

Fig. 4. Schematics of the assembly of particles with bedding angle of 30°: (a) initial state after generation; (b) at the end of isotropic consolidation. Boundary particles are highlighted.

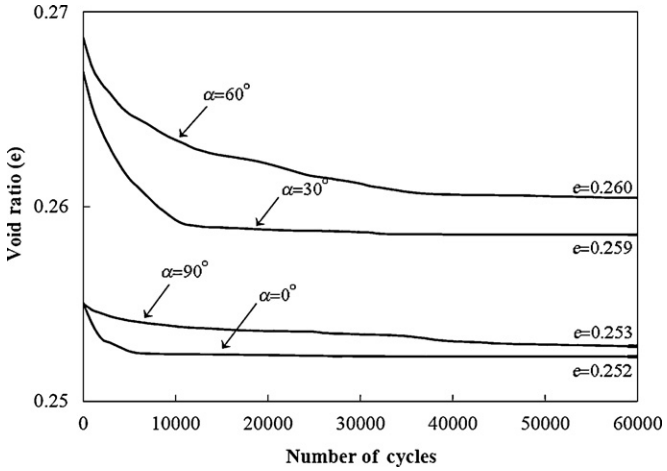

Fig. 5. Variation of void ratio with compaction cycles. Calculation cycles continue until a constant value of void ratio is reached for the particle assembly.

is reminded that despite the second stage, the inter-particle friction angle is turned on and equals 26.6° for isotropic compaction under constant confining pressure (second stage) and biaxial compression stage (see Table 2). This value corresponds to the quartz particles in natural soils measured in laboratory (Horn & Deere, 1962; Lambe & Whitman, 1969).

3.3. Simulation of biaxial compression tests

The biaxial compression test is carried out in such a way that the lateral stress imposed on the assembly along 1–1 axis (in the horizontal direction) is held constant (=300 kPa), while the assembly is loaded vertically with a constant displacement rate along the 2–2 axis (in the vertical direction). Thus, the sample deforms from being a circle to a horizontally elongated ellipse, as shown in Fig. 6. The biaxial compression test is continued to an axial strain of ε_{22} = 18%. Note that since the specimen is loaded in the vertical direction, the axial strain coincides with the 2–2 axis. The isotropic consolidation and biaxial compression stages of all four assemblies are simulated with the same group of DEM parameters as listed in Table 2. It is important to note that we have tentatively chosen the values of the parameters based on empirical trials. As explained before, we want to investigate the trends in the behavior as well as to compare the results obtained with experimental tests more qualitatively rather than quantitatively. The values of the parameters are also well consistent with those reported in DEM-based research in the literature (e.g., Mahmood & Iwashita, 2010; Mirghasemi et al., 1997; Sazzad & Suzuki, 2010). For physically measured and constrained values of the parameters, also see Pudasaini and Hutter (2007), Teufelsbauer et al. (2011), and Pudasaini, Hsiau, Wang, and Hutter (2005).

Table 2
DEM parameters used in this study.

DEM parameter	Value[a]
Time step increment (Δt)	1.2×10^{-5} s
Particle density	2500 kg/m^3
Confining pressure	300 kPa
Inter-particle friction angle (ϕ_μ)	26.6°
Cohesion between particles (C)	0.0 kPa
Normal spring constant (k_n)	2.0×10^8 N/m
Tangential spring constant (k_s)	2.0×10^8 N/m
Viscous translational damping coefficient (α_m)	10,000
Viscous rotational damping coefficient (α_I)	10,000

[a] Parameter values are not physically justified.

4. Simulation results

4.1. Observations

As mentioned before, the present paper only investigates the macroscopic mechanical behavior of inherently anisotropic assemblies and a microscopic investigation is out of the scope of the current study. However, it is known that the mechanical behavior of granular materials significantly depends on the events taking place among particles. In other words, better understanding of the macroscopic behavior of granular materials requires investigating microscopic happenings. Thus, let us take a brief look at the particles within the assemblies before the evolution of stress and deformability during loading is investigated. Fig. 6 presents inherently anisotropic specimens under both isotropically compacted and biaxially sheared conditions (at axial strain of 18%). As explained before, the specimens were prepared in such a way that the particles were orientated in specific directions, as can be verified by focusing on the magnified zones of the specimens shown in Fig. 6. By paying attention to the particle alignment in the sheared specimens, it is possible to find large vertically elongated voids generated among particles, which do not exist in non-sheared specimens. Oda et al. (1985) carried out biaxial tests on two-dimensional oval rods, showing large elongated voids generated in the assembly because of the buckling of columns made by particles along the major principal stress axis. These findings imply that apart from the initial condition in the fabric anisotropy, another rearrangement of particles has been induced in the assembly. They believed that this happening justifies the dilative behavior of granular assemblies. The same result was also reported by Oda et al. (1998) in plane strain tests on real sands (Toyoura and Ticino sands). By searching large voids and comparing them in all sheared samples in Fig. 6, it is clear that the specimen with the horizontal bedding angle $\alpha = 0°$ has more voids than the others. Thus, it is expected that this specimen should show higher degree of dilation, which is true as can be verified later by studying the variation of volumetric strain (see Section 4.3).

Referring to Fig. 6 again and comparing particle inclination inside the magnified zone for the cases before and after shearing, one can observe that the particles rotated more as the bedding angle increased. In order to quantitatively compare particle rotation for the whole assembly, the frequency distribution of particle orientation (the percentage of particles in every 10-degree increment of orientation) is depicted in Fig. 7 for all samples corresponding to the end of confining pressure as well as biaxial shear loading at the axial strain of 18%. Such form of frequency distribution is consistent with the experimental results reported by Oda et al. (1978). According to Fig. 7, the major direction of particle orientation remains more or less in the initial desired direction except for $\alpha = 60°$, for which the major orientation has moved to about 30°. However, the frequency distribution for all specimens is changed because of the shear loading; the value is significantly reduced corresponding to the initial bedding angle direction and in turn, the value related to other particle orientations is increased. This change in frequency distribution is much more evident within the assembly for $\alpha = 90°$. In such assembly, the frequency of particles corresponding to the initial orientation angle has decreased by 10% while the reduction for other samples hardly reaches 5%. The evolution observed in particles orientation during loading can be related to the global shear strength of assemblies. Such relation can be explained that the assembly with high change in particle inclination would show less shear strength, because the particles could not withstand applied forces and thus they have diverted from their initial orientation. As a consequence, it can be concluded that the specimen with $\alpha = 90°$ should have the lowest strength while the

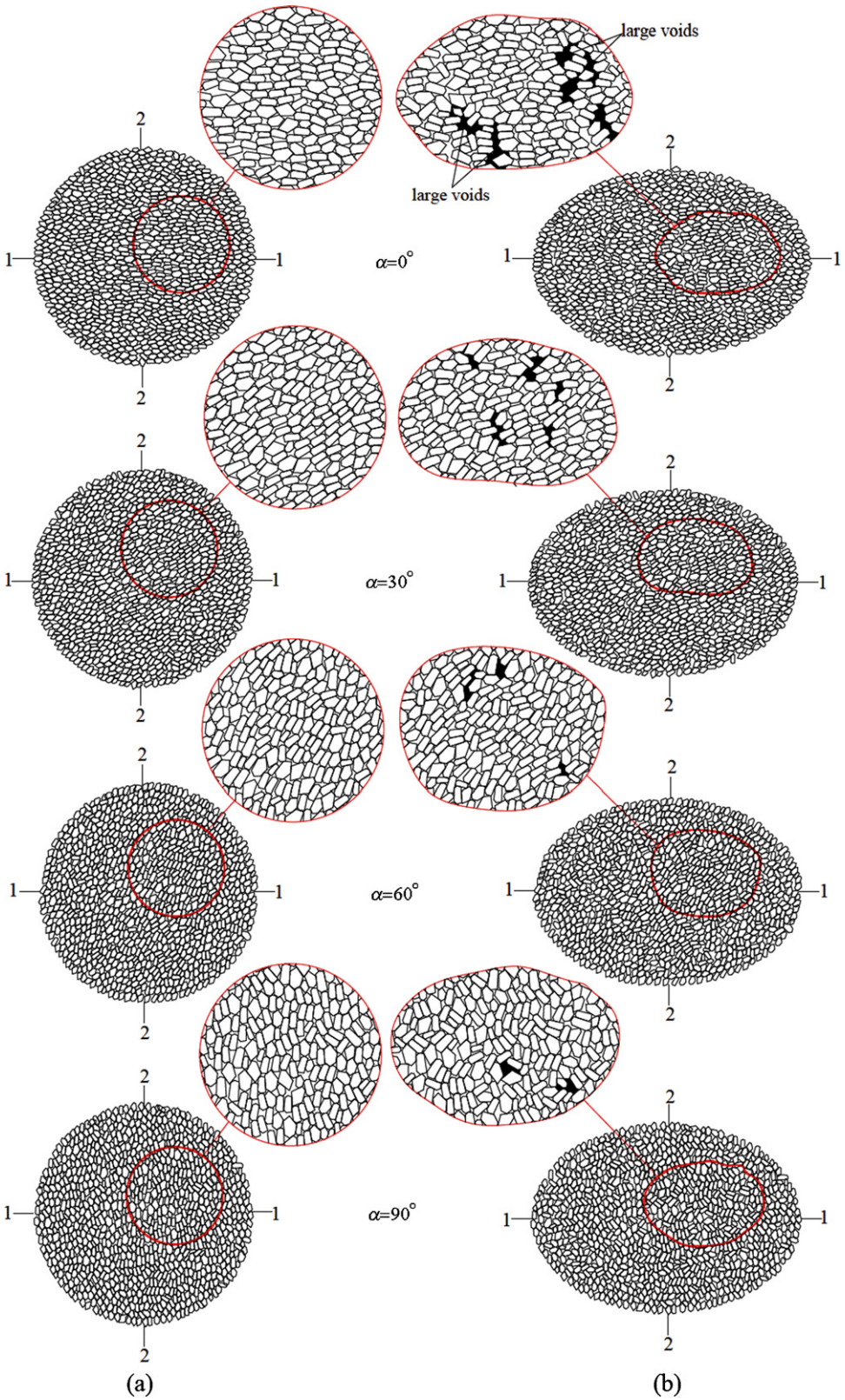

Fig. 6. Schematics of (a) isotropically consolidated assemblies; (b) biaxially sheared assemblies at the axial strain of 18%. Circular regions are magnified in order to better visualize the evolutions in the fabric. During shear loading, large voids are generated whose elongation is inclined toward the loading axis (2–2 axis).

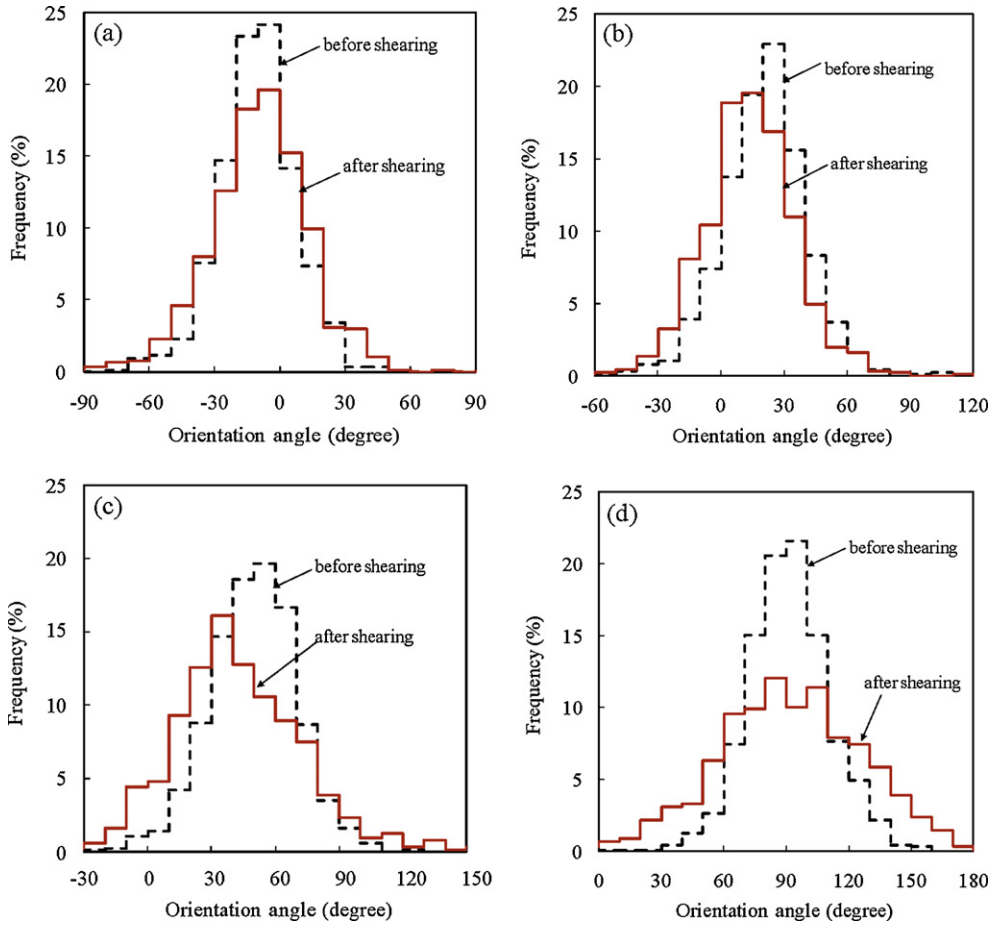

Fig. 7. Frequency distribution of particle orientation for isotropically consolidated and sheared specimens at $\varepsilon_{22} = 18\%$: (a) $\alpha = 0^\circ$; (b) $\alpha = 30^\circ$; (c) $\alpha = 60^\circ$; (d) $\alpha = 90^\circ$.

assembly with $\alpha = 0^\circ$, in which few particles have lost their initial direction, should show a high value in strength. This idea can be well evaluated by comparing the peak mobilized shear strength of specimens as will be discussed in the next section.

Apart from focusing on the particle orientation in such anisotropic fabrics, displacement pattern of particles is traced. Fig. 8 shows the displacement trajectories of all particles within all assemblies for four levels of axial strain. The trace lines are sketched with the same scale and proportional to the displacement magnitude. The global deformation observed in all assemblies shows the compression in the vertical direction and bulging in the lateral direction. This is more evident at larger levels of axial strain. However, the displacement patterns of particles are different from one assembly to the other, even at small axial strain levels ($\varepsilon_{22} = 3\%$), definitely because of the particle orientation with respect to the loading direction which leads to different global deformation. For instance, at axial strain of 7%, a high tendency in lateral deformation can be found in the assembly with $\alpha = 0^\circ$ in comparison with other assemblies. This implies that the assembly with $\alpha = 0^\circ$ should show a high degree of dilation in its behavior, which will be validated later by studying the variation of volumetric strain (Section 4.3). In this assembly, the long axis of most particles is oriented horizontally, and consequently, a loading step on particles imposes larger lateral deformation in comparison to other assemblies. At the same level of axial strain, except for the assemblies with $\alpha = 0^\circ$ and 90°, one can distinguish the initiation of two groups of particles with reverse displacement fields inside the assemblies with $\alpha = 30^\circ$ and 60°. The intermediate zone is known as a failure plane (shear band). The failure plane in the assembly with $\alpha = 30^\circ$ points upwards from left to right, while it is initiated in the reverse direction within the other assembly ($\alpha = 60^\circ$). At larger axial strain levels ($\varepsilon_{22} = 7\%$, 11%), the thickness of shear band in $\alpha = 30^\circ$ decreases, but the shear band in $\alpha = 60^\circ$ becomes wider. Within the assembly $\alpha = 0^\circ$, even at larger levels of deformation, no obvious shear band can be distinguished. Instead, different zones showing strain localization are distributed within the assembly. On the contrary, the formation of failure planes inside the assembly with $\alpha = 90^\circ$ is different: two crossing failure planes are detectable at axial strain of $\varepsilon_{22} = 11\%$, but only one of them remains at larger axial strain of $\varepsilon_{22} = 15\%$. Possibilities of different forms of shear bands in anisotropic sands were experimentally shown by Tatsuoka, Nakamura, Huang, and Tani (1990). Regarding the existence of two crossing shear bands for $\alpha = 90^\circ$, the high rotation of particles in the assembly is reminded, which indicates that the assembly has the tendency of having an isotropic fabric. As a consequence, it is expected that a symmetric pattern of shear band would be generated in the assembly. However, as the deformation of the assembly continues at high levels, one of the failure planes dominates and the other one diminishes. An extensive discussion on the occurrence and progression of strain localization in sands has been addressed by Desrues and Viggiani (2004).

4.2. Shear strength

In the present paper, the stress ratio q/p is considered as a representative of shear strength of granular assembly in which $q = (\sigma_{22} - \sigma_{11})/2$ is deviatoric stress and $p = (\sigma_{11} + \sigma_{22})/2$ is mean stress. σ_{11} and σ_{22} are average stresses applied over the boundary

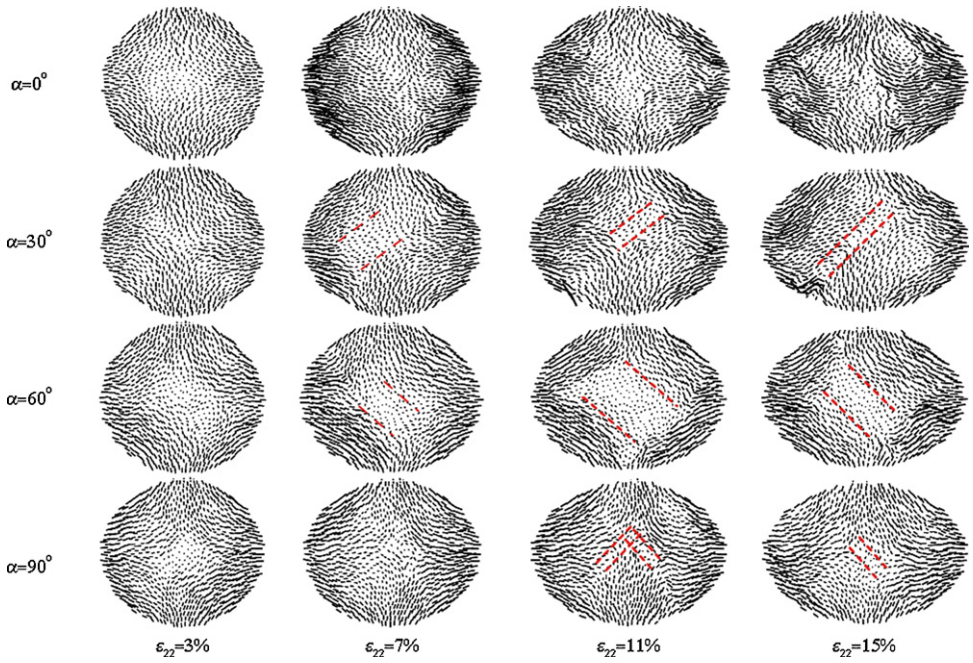

Fig. 8. Displacement fields of particles in assemblies during biaxial compression loading. The magnitude of particle traces are sketched at the same scale related to particle displacements. Red dash lines indicate the location of shear bands generated in the assembly. (For interpretation of the references to color in this figure legend, the reader is referred to the web version of the article.)

of the assembly along 1–1 and 2–2 directions, respectively. Since no shear stress is applied on the boundary, σ_{11} and σ_{22} can be regarded as minor and major principal stresses of the assembly. According to the Mohr–Coulomb failure criterion for cohesionless soils, i.e., $f=(\sigma_{22}-\sigma_{11})-\sin\phi(\sigma_{22}+\sigma_{11})=0$, the aforementioned stress ratio may be regarded as a function of internal friction angle by $\phi=\sin^{-1}(q/p)$. Fig. 9 presents the evolution of mobilized shear strength of assemblies with axial strain (ε_{22}) for bedding angles of $\alpha=0^\circ$, 30°, 60°, and 90°. The difference in the initial slope of the curves is related to the initial density, which corresponds to the void ratio at the end of isotropic compaction according to Fig. 5. From the onset of loading, the stress ratio of all samples increases rapidly until it reaches a maximum value and then the value decreases gradually to a constant limit. The stress ratio of the sample with $\alpha=90^\circ$ even tends to decrease as the shear deformation continues. The sample with $\alpha=0^\circ$ has the highest peak value in stress ratio, while the peak values for other samples reduce with increasing bedding angle. This trend remains true for the stress ratio in the post-peak part of the behavior.

In order to show more clearly the effect of inherent anisotropy on shear strength, the variation of maximum stress ratio with bedding angle (α) is presented in Fig. 10, which also depicts the results using oval particles by Mahmood and Iwashita (2010). It can be observed that the shear strength of the assemblies with polygonal particles is higher than that of the assembly with oval particles. However, dense specimens in both simulation groups were tested under the same condition of confining pressure of 300 kPa and similar DEM parameters, and thus, it seems that the only difference observed in shear strength originates from particle shape, since interlocking between polygonal particles is more than between oval particles. As a matter of fact, it is well known that the shear strength of granular materials increases with the angularity of particles.

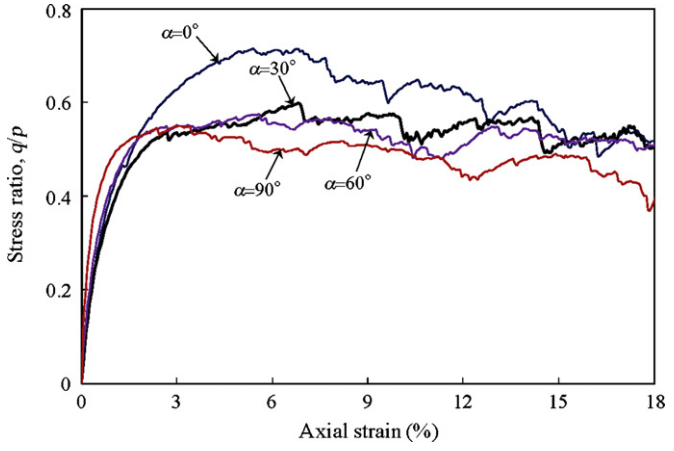

Fig. 9. Variation of mobilized shear strength (stress ratio) with axial strain for granular assemblies with different bedding angles.

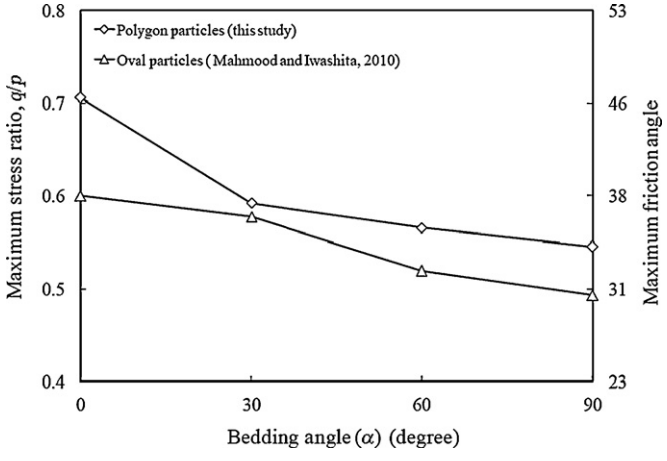

Fig. 10. Effect of initial anisotropic fabric on failure strength of granular assemblies. Results of the present work using angular particles are compared with those of Mahmood and Iwashita (2010) using oval particles.

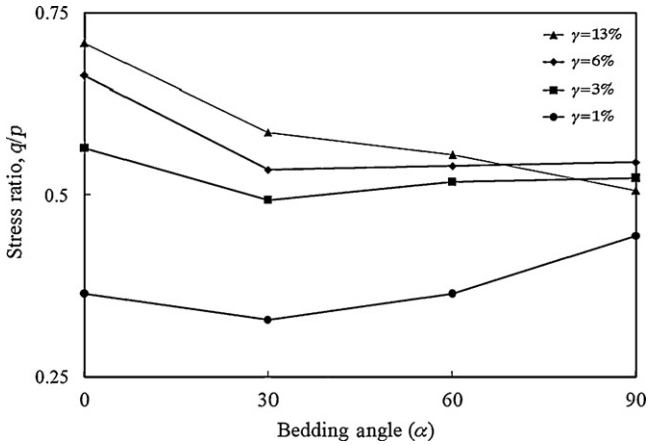

Fig. 11. Effect of bedding angle on shear strength for different shear strain levels based on DEM simulations.

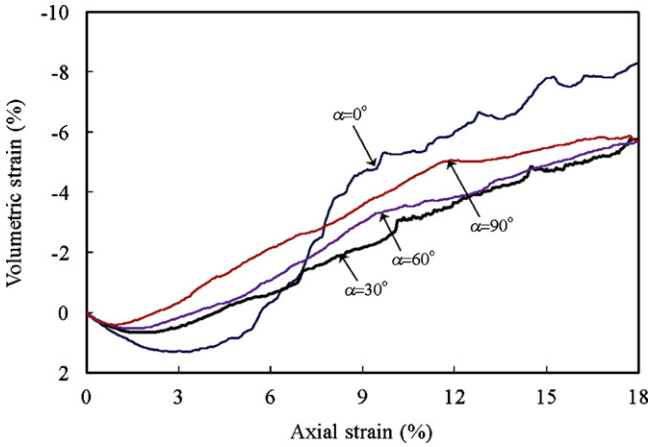

Fig. 12. Variation of volumetric strain with axial strain for all simulated assemblies.

By comparing the results obtained from these two series of numerical simulations (Fig. 10), it can be concluded that they obey the unique trend that increase in bedding angle decreases the shear strength of samples. These results are qualitatively similar to those of biaxial compression tests on oval photo-elastic rods (Oda et al., 1985) as well as triaxial and plane strain tests on real sand samples (Oda et al., 1978). There is, however, one difference in the obtained trend between triaxial (and current numerical simulations) and plane strain tests which indicates that the peak value of stress ratio becomes minimum at about $\alpha = 60^\circ$ in plane strain tests. In order to explain this discrepancy, it is firstly focused on the characteristics of the tests. Oda et al. (1978) declared that they observed shear planes parallel to bedding planes in plane strain tests, which was not the case for triaxial tests. Neither was this trend found in other researches by performing triaxial tests on anisotropic fabric samples (Arthur & Menzies, 1972; Arthur & Phillips, 1975). By investigating strain localization phenomenon in a number of both triaxial and plane strain tests, Desrues and Viggiani (2004) addressed that shear bands can be generated under certain situations and the occurrence of such phenomenon in a soil specimen was dependant on boundary condition and slenderness of the specimen. In addition, shear planes usually happen at smaller strain levels in plane strain tests and consequently, the peak stress ratio in plane strain tests generally pertain to small strains while the peak stress ratio in triaxial tests usually happen at larger strain levels. This fact has already been shown experimentally by performing both triaxial and plane strain tests on real sands (Oda et al., 1978). By paying attention to the strain level of peak stress ratio (Fig. 9) and the occurrence of shear planes in the numerical specimens (Fig. 8), it can be concluded that the numerical specimens behave more similarly close to triaxial samples rather than plane strain samples. To investigate the effect of strain level on this subject within the numerical specimens in the present study, the stress ratios of all samples are compared with each other at the same shear strains $\gamma = \varepsilon_{22} - \varepsilon_{11}$ and the result is sketched in Fig. 11. As can be seen, the bowl-shaped curve, as observed in plane strain tests, is obtained in small shear strains ($\gamma = 1\%$, 3%, and 6%), while the curve close to failure ($\gamma = 13\%$) does not obey this trend.

4.3. Dilation

The variation of volumetric strain $\varepsilon_v (= \varepsilon_{11} + \varepsilon_{22})$ versus axial strain for all samples is depicted in Fig. 12. All samples show dilative behavior during loading after initial contraction in volume. By comparing the graphs one another, it is interesting to observe that although the confining pressure and the initial density of all samples are the same, different inclinations of particles in the assemblies make distinguished effect on the manner how the samples to dilate. First, it is seen that at the initial loading, the assembly with $\alpha = 0^\circ$ behaves more contractively, while the sample with the bedding angle parallel to the major principal stress axis ($\alpha = 90^\circ$) shows a rapid change from contractive to dilative behavior (around $\varepsilon_{22} = 1\%$). In other words, the sample with $\alpha = 0^\circ$ has the most densification among others. Second, by following the variation of volumetric strain, it is seen that at larger axial strain level ($\varepsilon_{22} > 7\%$), the sample with horizontal bedding angle ($\alpha = 0^\circ$) has the highest dilative behavior. This trend agrees well with the fact that the volume expansion increases as the stress ratio increases. These observations in the volume change can be also found in experimental tests (Miura et al., 1986; Pudasaini & Hutter, 2007) as well as numerical simulations using oval/elliptical-shaped particles (Mahmood & Iwashita, 2010). In addition, using DEM with oval particles, Sazzad and Suzuki (2010) have shown such trend in deformational behavior of granular assemblies in small strain and large strain levels by cyclic and monotonic loadings, respectively.

In order to investigate the effect of particle shape on the initial densification of inherently anisotropic assemblies, the volumetric strain of all samples at the phase transformation point (from contractive to dilative behavior) is drawn versus the bedding angle in Fig. 13 for both series of samples with polygonal and oval particles. As can be seen, the samples tend to be less densified as the

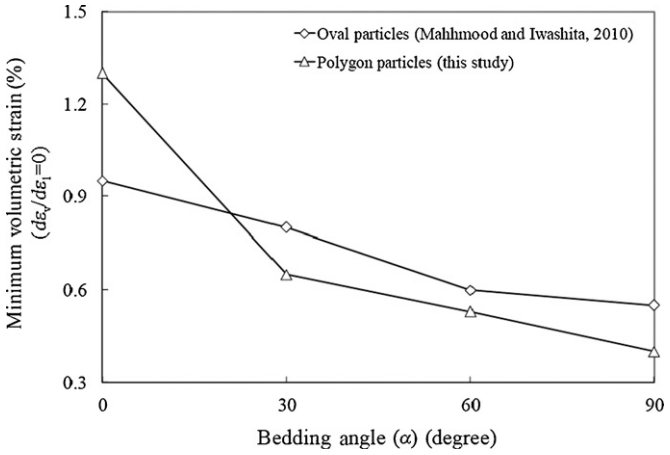

Fig. 13. Variation of minimum volumetric strain with bedding angle for simulated assemblies with oval and polygonal particles.

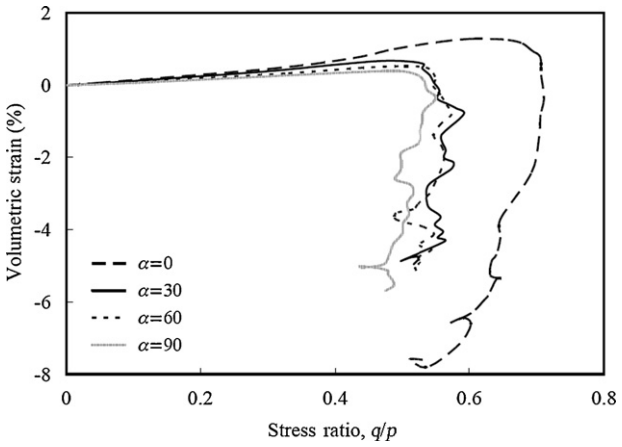

Fig. 14. Relationship between shear strength and dilatancy for different inherently anisotropic assemblies simulated in this paper.

bedding angle increases regardless of containing oval or angular particles. Such behavior corresponds to the generation of column-like structures made up of particles and their following buckling phenomenon which results in dilative behavior. Since the generation and collapse of such columns happen sooner among unstable particles, it is justifiable that the sample with $\alpha = 90^\circ$, in which there are the least stable particles (having more rotation), shows the least densification. Furthermore, it can be observed, in Fig. 13, that the assemblies with angular particles tend to have less densification in comparison with those with oval particles, which is because of the more interlocking resistance between angular particles than that between oval particles.

In order to show clearly the relationship between stress ratio and volume change, the variation of volumetric strain with stress ratio is presented in Fig. 14. This graph distinctively indicates that not only a direct relationship exists between stress ratio and dilation, but also the inherent anisotropy has great influence on both shear strength and dilatancy regime. This tendency agrees well with the experimental results presented by Miura et al. (1986). In this regard, based on measuring the stress ratio at which the behavior changes from contractive to dilative, Miura et al. (1986) expressed that the stress ratio at zero volumetric strain increment is a parameter independent of sand fabrics (see also Miura & Toki, 1984). To investigate such idea, the stress ratios at the phase transformation point ($d\varepsilon_v/d\gamma = 0$) are assessed for DEM simulations and the results are sketched in Fig. 15 along with other experimental and numerical tests. Surprisingly, it can be found out that both experimental and numerical tests reveal that the stress ratio belonging to zero volumetric strain increment is around a constant value and equals $q/p = 0.5$, although it is slightly higher for all DEM simulations at $\alpha = 0^\circ$. Note that the actual applied stress and strain (boundary) conditions differ from 100 to 300 kPa and particle geometry and configurations are also different. The value of measured stress ratio (0.5) might be related to the inter-particle friction angle since this parameter in DEM simulations ($\phi_\mu = 26.6^\circ$) is considered the same as the inter-particle friction angle of natural sands (Horn & Deere, 1962; Lambe & Whitman, 1969). This coincidence should be investigated more and further studies are needed for evaluation.

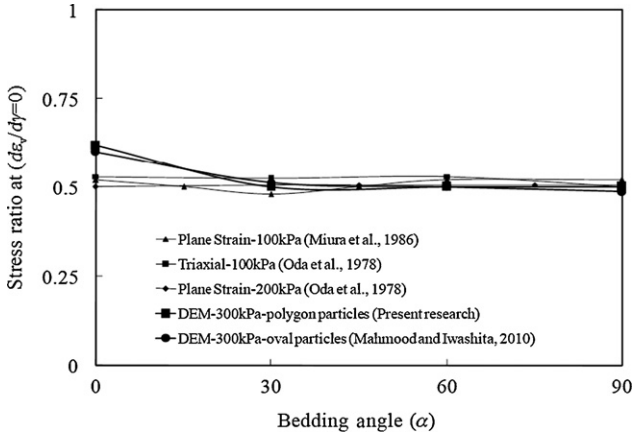

Fig. 15. Stress ratio at maximum contraction volume for different numerical as well as experimental tests. Note that the actual applied stress and strain (boundary) conditions differ from 100 to 300 kPa and particle geometry and configurations are also different.

5. Conclusions

By using the discrete element method (DEM), numerical simulations were carried out to investigate the effect of inherent anisotropy on the macroscopic behavior of granular assemblies. To this aim, several numerical biaxial compression tests were performed on granular assemblies, in which the particles geometry was considered as convex polygons.

The behavior was studied in terms of shear strength and compressibility. Simulations show that the assembly, in which the major principal stress direction is coaxial with the bedding angle of particles ($\alpha = 90^\circ$), has the least shear strength, and vice versa. Also, inherent anisotropy can change the tendency of the assembly to deform, that is, the increase in bedding angle reduces the initial compressibility of the sample. However, there is a reverse order between the degree of the resulting dilative behavior and the bedding angle. In other words, the assembly with the bedding angle perpendicular to the major principal stress axis ($\alpha = 0^\circ$) dilates more than other assemblies.

By comparing the results of the simulations of this study using convex polygons with those of other series of simulations using oval particles, it was observed that the shear strength was higher for polygonal particles. This is due to the angularity of polygons which increases the interlocking resistance between particles. Due to the same reason, the compressibility of polygonal particles was found to be less than that of oval particles.

The difference observed in the behavior of inherently anisotropic assemblies under the same initial conditions (density and stress level) can be justified by focusing on the fabric evolution, where the highest shear strength and dilation occur in the assembly with the least change in particle inclination. Moreover, it was found that the dilatancy of the granular assembly is a consequence of large voids generated among particles, as was observed and proved in laboratory.

Comparisons between simulation results and observations from experimental tests qualitatively show good agreement for stress ratio and bedding angles. It should be emphasized that the analysis performed in this study on granular materials was two-dimensional and could only allow us to have a better understanding of the mechanism of granular materials more qualitatively rather than quantitatively. Consequently, the results presented here need to be confirmed with a three-dimensional analyses and consistent simulations performed with more physically meaningful parameters.

Acknowledgements

The present work reported in this paper was supported by Research Deputy of Ferdowsi University of Mashhad. The provided

grant (No. 16759-03/12/89) for this project is gratefully acknowledged.

References

Al-Hattamleh, O., Muhunthan, B., & Shalabi, F. (2009). Numerical simulation of fabric anisotropy and strain localization of sand under simple shear. *International Journal for Numerical and Analytical Methods in Geomechanics*, *33*, 1255–1275.

Arthur, J. R. F., & Menzies, B. K. (1972). Inherent anisotropy in a sand. *Géotechnique*, *22*(1), 115–128.

Arthur, J. R. F., & Phillips, A. B. (1975). Homogeneous and layered sand in triaxial compression. *Géotechnique*, *25*(4), 799–815.

Bathurst, R. J. (1985). *A study of stress and anisotropy in idealized granular assemblies* (Doctoral dissertation). Queen's University, Kingston.

Bowman, E. T., Soga, K., & Drummond, W. (2011). Particle shape characterization using Fourier descriptor analysis. *Géotechnique*, *51*(6), 545–554.

Christoffersen, J., Mehrabadi, M. M., & Nemat-Nasser, S. (1981). A micromechanical description of granular material behavior. *Journal of Applied Mechanics, Transactions of the ASME*, *48*(2), 339–344.

Cundall, P. A., & Strack, O. D. L. (1979). A discrete numerical model for granular assemblies. *Géotechnique*, *29*(1), 47–65.

Dafalias, Y. F., Papadimitriou, A. G., & Li, X. S. (2004). Sand plasticity model accounting for inherent fabric anisotropy. *Journal of Engineering Mechanics*, *130*(11), 1319–1333.

Desrues, J., & Viggiani, G. (2004). Strain localization in sand: An overview of the experimental results obtained in Grenoble using stereophotogrammetry. *International Journal for Numerical and Analytical Methods in Geomechanics*, *28*, 279–321.

Horn, H. M., & Deere, D. U. (1962). Frictional characteristics of minerals. *Géotechnique*, *12*, 319–335.

Houlubec, I., & D'Appolonia, E. (1973). Effect of particle shape on the engineering properties of granular soils. In *Proceedings of symposium on evaluation of relative density* Los Angeles, USA.

Jensen, R. P., Bosscher, P. J., Plesha, M. E., & Edil, T. B. (1999). DEM simulation of granular media–structure interface: Effects of surface roughness and particle shape. *International Journal for Numerical and Analytical Methods in Geomechanics*, *23*(6), 531–547.

Lambe, T. W., & Whitman, R. V. (1969). *Soil mechanics*. New York: John Wiley and Sons.

Mahmood, Z., & Iwashita, K. (2010). Influence of inherent anisotropy on mechanical behavior of granular materials based on DEM simulations. *International Journal for Numerical and Analytical Methods in Geomechanics*, *34*, 795–819.

Mirghasemi, A. A., Rothenburg, L., & Matyas, E. L. (1997). Numerical simulations of assemblies of two-dimensional polygon-shaped particles and effects of confining pressure on shear strength. *Soils and Foundations*, *37*(3), 43–52.

Mirghasemi, A. A, Rothenburg, L., & Matyas, E. L. (2002). Influence of particle shape on engineering properties of assemblies of two-dimensional polygon-shaped particles. *Géotechnique*, *52*(3), 209–217.

Miura, K., Miura, S., & Toki, S. (1986). Deformation behavior of anisotropic dense sand under principal stress axes rotation. *Soils and Foundations*, *26*(1), 36–52.

Miura, S., & Toki, S. (1984). Elastoplastic stress–strain relationship for loose sands with anisotropic fabric under three-dimensional stress conditions. *Soils and Foundations*, *24*(2), 43–57.

Ng, T. (2004). Macro- and micro-behaviors of granular materials under different sample preparation methods and stress paths. *International Journal of Solids and Structures*, *41*(21), 5871–5884.

Nouguier-Lehon, C., Cambou, B., & Vincens, E. (2003). Influence of particle shape and angularity on the behaviour of granular materials: A numerical analysis. *International Journal for Numerical and Analytical Methods in Geomechanics*, *27*, 1207–1226.

Oda, M. (1972). Initial fabrics and their relations to mechanical properties of granular material. *Soils and Foundations*, *12*(1), 18–36.

Oda, M. (1993). Inherent and induced anisotropy in plasticity theory of granular soils. *Mechanics of Materials*, *16*, 35–45.

Oda, M., Kazama, H., & Konishi, J. (1998). Effects of induced anisotropy on the development of shear bands in granular materials. *Mechanics of Materials*, *28*, 103–111.

Oda, M., Koishikawa, I., & Higuchi, T. (1978). Experimental study of anisotropic shear strength of sand by plane strain test. *Soils and Foundations*, *18*(1), 25–38.

Oda, M., Konishi, J., & Nemat-Nasser, S. (1982). Experimental micromechanical evaluation of strength of granular materials: Effects of particle rolling. *Mechanics of Materials*, *1*, 269–283.

Oda, M., Nemat-Naser, S., & Konishi, J. (1985). Stress-induced anisotropy in granular masses. *Soils and Foundations*, *25*(3), 85–97.

Peña, A. A, García-Rojo, R., & Herrmann, H. J. (2007). Influence of particle shape on sheared dense granular media. *Granular Matter*, *9*, 279–291.

Peña, A. A., McNamara, S., Lind, P. G., & Herrmann, H. J. (2009). Avalanches in anisotropic sheared granular media. *Granular Matter*, *11*, 243–252.

Pudasaini, S. P. (2011). Some exact solutions for debris and avalanche flows. *Physics of Fluids*, *23*(4), 043301.

Pudasaini, S. P., Hsiau, S.-S., Wang, Y., & Hutter, K. (2005). Velocity measurements in dry granular avalanches using particle image velocimetry-technique and comparison with theoretical predictions. *Physics of Fluids*, *17*(9), 093301.

Pudasaini, S. P., & Hutter, K. (2007). *Avalanche dynamics: Dynamics of rapid flows of dense granular avalanches*. New York: Springer.

Pudasaini, S. P., Hutter, K., Hsiau, S.-S., Tai, S.-C., Wang, Y., & Katzenbach, R. (2007). Rapid flow of dry granular materials down inclined chutes impinging on rigid walls. *Physics of Fluids*, *19*(5), 053302.

Pudasaini, S. P., & Kröner, C. (2008). Shock waves in rapid flows of dense granular materials: Theoretical predictions and experimental results. *Physical Review E*, *78*(4), 041308.

Rothenburg, L., & Selvadurai, A. P. S. (1981). A micromechanical definition of the Cauchy stress tensor for particulate media. In *Proceedings of the international symposium on the mechanical behavior of structured media, part B* Ottawa, Canada.

Sallam, A. M. (2004). *Studies on modeling angular soil particles using the discrete element method* (Doctoral dissertation). University of South Florida, USA.

Sazzad, M. M., & Suzuki, K. (2010). Micromechanical behavior of granular materials with inherent anisotropy under cyclic loading using 2D DEM. *Granular Matter*, *12*, 597–605.

Seyedi Hosseininia, E., & Mirghasemi, A. A. (2006). Numerical simulation of breakage of two-dimensional polygon-shaped particles using discrete element method. *Powder Technology*, *166*, 100–112.

Seyedi Hosseininia, E., & Mirghasemi, A. A. (2007). Effect of particle breakage on the behavior of simulated angular particle assemblies. *China Particuology*, *5*, 328–336.

Shodjaa, H. M., & Nezami, E. G. (2003). A micromechanical study of rolling and sliding contacts in assemblies of oval granules. *International Journal for Numerical and Analytical Methods in Geomechanics*, *27*, 403–424.

Sitharam, T. G. (1991). *Numerical simulation of hydraulic fracturing in granular media* (Doctoral dissertation). University of Waterloo, Waterloo, Canada.

Tatsuoka, F., Nakamura, S., Huang, C.-C., & Tani, K. (1990). Strength anisotropy and shear band direction in plane strain tests of sand. *Soils and Foundations*, *30*(1), 35–54.

Teufelsbauer, H., Wang, Y., Pudasaini, S. P., Borja, R. I., & Wu, W. (2011). DEM simulation of impact force exerted by granular flow on rigid structures. *Acta Geotechnica*, *6*(3), 119–133.

Ting, J. M., & Meachum, L. R. (1995). Effect of bedding plane orientation on the behavior of granular systems. *Mechanics of Materials with Discontinuities and Heterogeneities*, *201*, 43–57.